Supporting Online Material for

Mechanical Control of Spin States in Spin-1 Molecules and the Underscreened Kondo Effect

J. J. Parks, A. R. Champagne, T. A. Costi, W. W. Shum, A. N. Pasupathy, E. Neuscamman, S. Flores-Torres, P. S. Cornaglia, A. A. Aligia, C. A. Balseiro, G. K.-L. Chan, H. D. Abruña, D. C. Ralph*

*To whom correspondence should be addressed. E-mail: ralph@ccmr.cornell.edu

Published 11 June 2010, *Science* **328**, 1370 (2010)
DOI: 10.1126/science.1186874

This PDF file includes:

Supporting Online Material

Contents

S1. Materials and methods

To make the mechanically controllable break-junction devices, we start by fabricating continuous gold lines (32 nm thick, 500 nm long, and with a 50 nm-wide constriction) suspended 40 nm above a 200 μm-thick Si wafer [S1, S2]. Fabrication of the fixed-electrode devices follows procedures described in Refs. [S3, S4]. To incorporate the molecules into either type of device, we clean unbroken wires in an oxygen plasma to remove organic contaminants and then immerse the samples into a <0.1 mM solution of Co(tpy-SH)$_2$ with PF_6^- counterions in acetonitrile, allowing the thiol end groups of the molecules to attach to the gold. We synthesized the molecules by the process described in Ref. [S3] and purified them by flash chromatography using an alumina column, yielding a final purity >99% prior to deposition. After the sample chip is removed from the molecular solution, excess solution is blown off with nitrogen gas and the samples are cooled to low temperature (T = 1.6 K). We then use electromigration [S5] to create a molecular-scale break in the wires. The electrode motion is calibrated [S6] from the tunneling conductance of junctions lacking any added molecules.

After electromigration, we observed a peak in dI/dV at $V = 0$, characteristic of the Kondo effect, in approximately 14% of ~250 mechanically controllable devices and 18% of ~200 fixed-electrode

devices made with Co(tpy-SH)$_2$ solution. Approximately 3% of devices exhibited a high-resistance Coulomb blockade characteristic without a Kondo feature, and the rest had featureless dI/dV vs. V traces indicative of simple tunneling. Among the devices with a conductance feature near zero-bias, at the initial electrode spacing ~20% of the adjustable devices and ~10% of the fixed-electrode devices had split peaks (suggesting that the molecule is already stretched); the peak positions ranged up to $|V| = 5$ mV. Four adjustable devices possessed sufficient stability to repeatedly observe the transition between split and unsplit peaks as a function of stretching. No devices showed a decrease in the Kondo splitting with stretching; two showed a zero-bias Kondo peak that did not split with stretching (see Section S5). Among 47 adjustable and 24 fixed-electrode devices prepared as control samples with acetonitrile alone, none contained a zero-bias peak in dI/dV and only one exhibited Coulomb blockade.

S2. Additional devices for which the Kondo peak splits with stretching

In Fig. S1 we show data for two devices (Devices I and J), in addition to the two described in the main text, that display a splitting of the Kondo peak with stretching. While we were able to tune from a single Kondo peak to split Kondo peaks and then return to a single peak on a subsequent reverse scan with Devices I and J, these junctions were not sufficiently stable to make detailed temperature and magnetic field measurements.

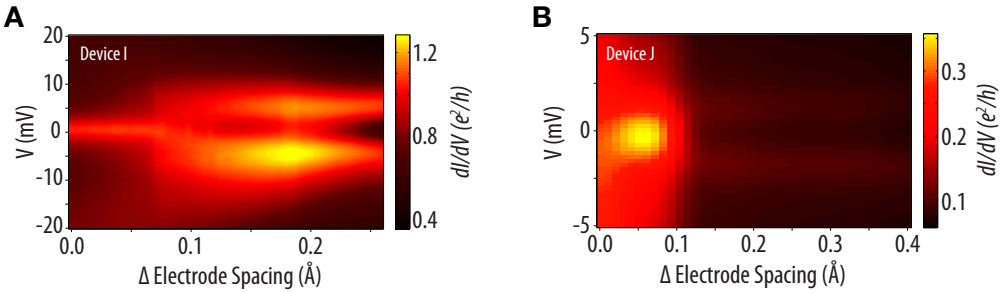

Figure S1: Two additional devices that showed a splitting of the Kondo peak with stretching.

S3. Fitting to Numerical Renormalization Group (NRG) predictions for $G(T)$

NRG calculations for Kondo-assisted tunneling via an impurity of spin S coupled to a *single* screening channel predict the temperature dependence of the conductance in the form of a discrete set of points, $G/G(0)$ as a function of T [S7]. The calculations were carried out with a logarithmic discretization parameter $\Lambda = 1.5$ [S8] and retaining 1700 states per NRG iteration. In order to fit experimental data to these NRG predictions, we first approximate the NRG results by a set of analytical fitting functions having the scaling form $G_S^*(T) = G(0)\, f_S(T/T_K)$, where T_K is defined

so that $G(T_K) \equiv G(0)/2$, as was done in Refs. [S8, S9]. We do not wish to imply any physical significance to the form of these fitting functions; they are merely an attempt to approximate the NRG results with a minimum number of adjustable parameters. We use as a starting point the phenomenological Goldhaber-Gordon form [S9] for the temperature dependence of the spin-1/2 Kondo effect

$$g_S(T/T_K) = \left[1 + \left(\frac{T}{T'_K}\right)^{\xi_S}\right]^{-\alpha_S}, \tag{S1}$$

but we relax the condition $\xi_S = 2$ (applicable for a fully screened Kondo effect) since for $S > 1/2$, the ground state of an underscreened Kondo system is not a Fermi liquid. Note that the quantity T'_K of Eq. (S1) is related to the actual Kondo temperature by

$$T'_K = \frac{T_K}{(2^{1/\alpha_S} - 1)^{1/\xi_S}}. \tag{S2}$$

We find that as the temperature is reduced, functions of the form in Eq. (S1) saturate more quickly to the maximum value of 1 than do the NRG results for the underscreened Kondo effects – the calculated conductance is not yet saturated at the lowest temperatures $T/T_K \sim 10^{-4}$ available in the results. To better account for this slow saturation, we find over many decades of temperature around T_K that good fits to the NRG results can be obtained by including a small offset parameter Δ_S, such that for our phenomenological scaling functions we use the form

$$G^*_S(T) = G(0) \underbrace{\left[(1 - \Delta_S)\, g_S(T/T_K) + \Delta_S/2\right]}_{f_S(T/T_K)}. \tag{S3}$$

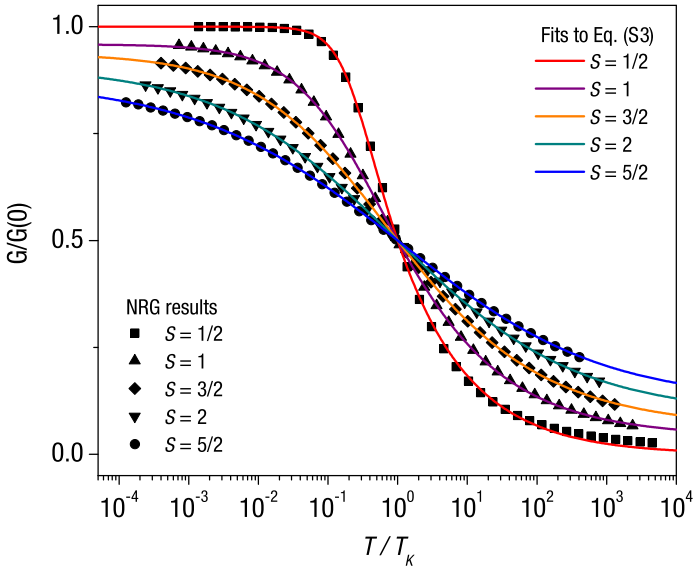

Figure S2: Fits of NRG conductances $G(T)$ to Eq. (S3) for S = 1/2, 1, 3/2, 2, and 5/2.

In the above, the coefficient $(1 - \Delta_S)$ helps to account for the incomplete saturation of conductance for underscreened Kondo effects at the lowest temperatures available in the NRG results, and the second term $\Delta_S/2$ is added to retain consistency with the definition of the Kondo temperature; one can verify by inspection that the term allows the condition $G_S^*(T_K) = G(0)/2$ to be satisfied. The reader should not be confused by the fact that $G_S^*(0) \neq G(0)$, because in our fits we will be concerned only about temperatures within several decades of T_K, not with the ultimate low-temperature limit.

In Fig. S2, we show fits of Eq. (S3) to the NRG data for S = 1/2, 1, 3/2, 2, and 5/2, where ξ_S, α_S, and Δ_S are used as fitting parameters. The case of S = 1/2 is an exception – here we fixed $\xi_S = 2$ and $\Delta_S = 0$ as was done in Ref. [S9]. The fitting parameters are summarized in Table S1. The NRG results are very well described by Eq. (S3) for over 7 decades in T/T_K, with particularly good agreement in the regime $10^{-3}\ T_K \lesssim T \lesssim T_K$, which is the most relevant for comparison to our experiments. In order to fit the predictions of the Kondo models for different spins S to our experimental data, we employ Eq. (S3) keeping fixed the values of the parameters ξ_S, α_S, and Δ_S as listed in Table S1, and use $G(0)$ and T_K as the only adjustable fitting parameters. In fitting to the experimental data, we did not include a background term as an adjustable parameter in Eq. (S3).

Table S1: Fitted parameters determined by using Eq. (S3) to approximate the NRG predictions for the temperature dependence of conductance for a Kondo impurity of spin S with a single screening channel (giving a fully screened Kondo model for $S = 1/2$ and underscreened for $S > 1/2$).

Spin	ξ_S	α_S	$\Delta_S/2$
$S = 1/2$	2	0.220 ± 0.005	0
$S = 1$	0.745 ± 0.009	0.506 ± 0.009	0.041 ± 0.001
$S = 3/2$	0.483 ± 0.004	0.670 ± 0.008	0.062 ± 0.002
$S = 2$	0.349 ± 0.004	0.912 ± 0.013	0.093 ± 0.002
$S = 5/2$	0.288 ± 0.004	1.116 ± 0.023	0.124 ± 0.003

S4. Fitting the measured $G(T)$ to Kondo scaling predictions for different values of S, for all samples

We measured the detailed temperature dependence of the unsplit Kondo signal in ten Co(tpy-SH)$_2$ devices, including two devices with adjustable electrodes (A and B) and eight with fixed electrodes. For each set of data $G(T)$ we performed fits to the predicted scaling curves (Eq. (S3)) for the fully screened S = 1/2 Kondo model and the underscreened S = 1 and 3/2 Kondo models, with two fitting parameters for each fit, the zero-temperature conductance $G(0)$ and the Kondo temperature T_K. (To be clear, different best-fit values of $G(0)$ and T_K were determined for each

A. Underscreened $S = 1$ scaling for seven different Co(tpy-SH)$_2$ devices

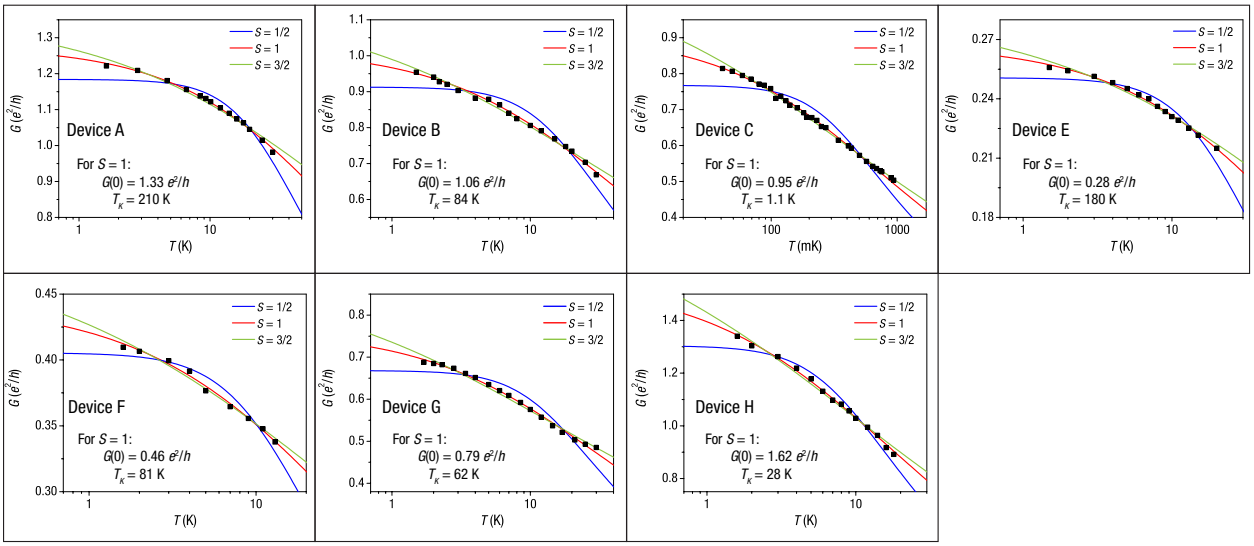

B. $S = 1/2$ scaling for two Co(tpy-SH)$_2$ devices (likely a different charge state of the molecule)

C. Ambiguous scaling

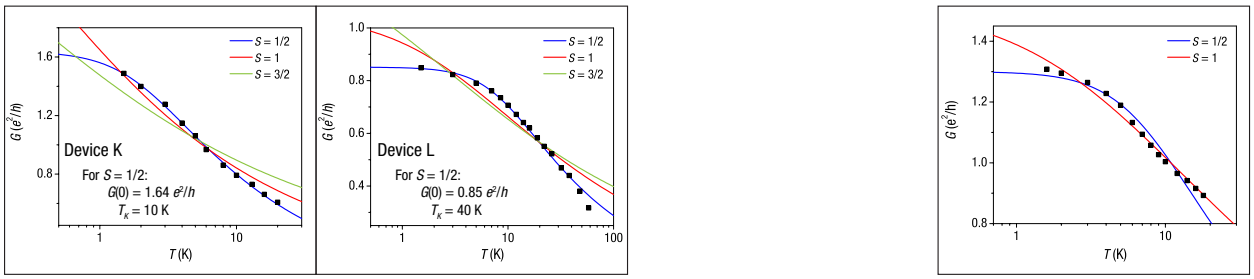

D. $S = 1/2$ scaling from previously studied C_{60} devices

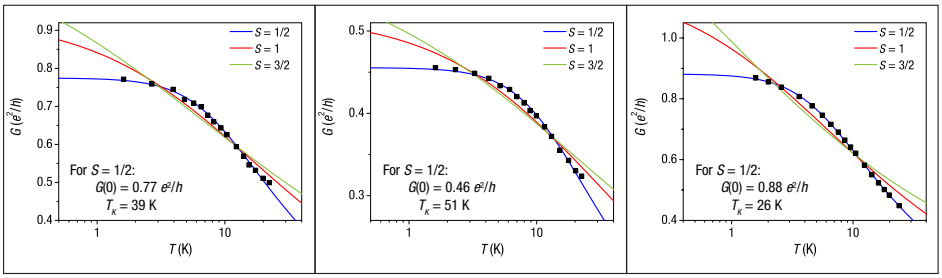

Figure S3: Fits of $G(T)$ to Eq. (S3) for ten Co(tpy-SH)$_2$ devices. (**A**) Seven devices show a temperature scaling that deviates from the $S = 1/2$ fully screened Kondo prediction, and is instead in good agreement with the underscreened $S = 1$ Kondo effect. (**B**) Data from 2 devices are consistent with a spin-1/2 Kondo effect, likely arising from a molecule with a Co^{2+} charge state. (**C**) One device did not unambiguously fit any of the predicted forms for a single Kondo impurity. (**D**) $S = 1/2$ scaling observed in previously studied C_{60} devices [S2].

value of S.) The results are shown in Fig. S3 for all ten unstretched Co(tpy-SH)2 devices, seven of which showed $S = 1$ scaling, two of which showed $S = 1/2$ scaling, and one device that showed ambiguous scaling. For comparison, we also show the same analysis for three previously studied C_{60} devices with $S = 1/2$ [S2].

The first conclusion we can draw is that generally there is no ambiguity in distinguishing between realizations of the fully screened $S = 1/2$ Kondo effect and the underscreened Kondo effects, because the underscreened models predict a *very* slow approach to saturation with decreasing temperature, whereas the fully screened models saturate rapidly at low T. All of the devices we have measured, except for the one exception noted, give excellent fits to either the fully screened $S = 1/2$ curve or the underscreened curves, with a very poor fit to the other. From this we conclude, first, that the seven devices shown in Fig. S3A have $S \geq 1$. That the temperature dependence for each of these samples can be fit well with a single value of T_K indicates that we measure current flow via a single molecule in each device.

Distinguishing between the different models of the underscreened Kondo effect (*e.g.*, $S = 1$ vs. 3/2) based solely on the temperature dependence is more challenging because the scaling curves are similar, with most of the difference due to a few points at the high and low temperature ends of the fitting ranges. However, all seven of the samples that exhibit an underscreened characteristic exhibit better agreement with the $S = 1$ curve than with $S = 3/2$ or higher spin. As discussed in the main text, the magnetic field dependence of the Kondo peak splitting provides additional confirmation that $S = 1$.

For the devices in Fig. S3B that show $S = 1/2$ scaling, our interpretation is that the molecule in these devices likely retained a different charge state (*e.g.*, Co^{2+}) than the molecules exhibiting the underscreened Kondo effect. The presence or absence of nearby counterions or other charged impurities, or differences in local work functions for the disordered gold electrodes, could easily lead to large differences in the local electrostatic potential at the position of the molecule through which current flows, thereby providing in effect a local gate to change its charge state. The Co^{2+} state should have a ground state spin $S = 1/2$ at low temperature [S10], which can produce the conventional fully screened $S = 1/2$ Kondo effect.

The one device showing a temperature dependence different from both the $S = 1$ and $S = 1/2$ predictions (Fig. S3C) may possibly be explained by conduction through two molecules in parallel, with different Kondo temperatures or possibly to being in a mixed-valence, rather than a purely Kondo, regime [S11].

S5. Two Co(tpy-SH)$_2$ devices did not show a splitting of the Kondo peak with stretching

Increasing the electrode spacing did not result in a splitting of the Kondo peak in two devices that we measured. The dI/dV of one such device as a function of increasing electrode spacing is shown in Fig. S4. Stretching modifies the height and width of the Kondo peak, but the peak does not split. This behavior might be explained in several ways. One is that the molecule may not be strongly bonded to both electrodes so that electrode displacement does not significantly stretch the metal complex. The effect of electrode displacement in this case would be only to reduce the Kondo conductance and temperature without significantly affecting the symmetry of the molecule [S2]. A second possibility is that the spin state of the molecule for these two devices is $S = 1/2$ (*i.e.*, in the Co^{2+} state), as discussed above.

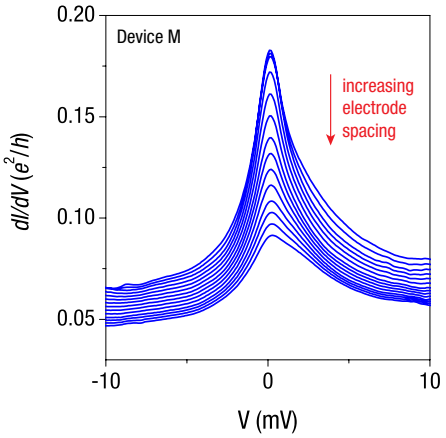

Figure S4: *dI/dV* traces with increasing electrode spacing for a device at $T = 1.6$ K, which did not show a splitting of the Kondo peak with stretching.

S6. Calculations of zero-field splittings

We carried out calculations of the zero-field splitting for the isolated molecule spin-triplet state within the DFT coupled-perturbed spin-orbit coupling formalism [S13], as implemented in ORCA [S14]. Precise reproduction of the observed experimental D values is challenging because of the dependence on the molecular environment. It is sensitive in particular to the overall spin density on the cobalt, which gives some insight into the mechanism of how the variation in D may be affected at a microscopic level. For the molecule at equilibrium geometry, we find that the zero-field splitting is ~0.1 meV, consistent with the expectation of a small value for nearly octahedral symmetry. As we tune the exchange contribution in the density functional to shift the spin density onto the cobalt atom, the zero-field splitting can increase. For an exchange contribution that produces a similar magnetic moment (1.2 Bohr magnetons) on the cobalt atom as observed in LDA + U calculations on the molecule-electrode system, we obtain a D of 2.7 meV (using 80% exchange).

This is of the same sign and similar in magnitude to the splittings observed in the experiment. The amount of exchange required is quite high, but the primary effect (to shift spin density onto the cobalt atom) might arise in the experiment from attachment to the electrodes.

We also tried to obtain the dependence of D on molecular geometry. This was complicated by numerical artifacts arising from the solution of the coupled-perturbed equations treatment. Redistribution of the unpaired electrons between the Co ion and the ligands might also contribute to changes in the magnitude of D as the metal-ligand coupling changes. However, variations on the order of 1 meV were calculated.

S7. Spin energy levels as a function of magnetic field for $S = 3/2$

In Figures 4A and 4B of the main manuscript, we plotted the spin energy levels and the Kondo peak position as a function of magnetic field for several different field angles relative to the stretching axis $\hat{z}$, for a simple spin Hamiltonian $H = -g\mu_B \mathbf{B} \cdot \mathbf{S} + DS_z^2$ with $S = 1$ in the presence of a spin anisotropy energy $D > 0$. In Fig. S5 we plot the results of the same model Hamiltonian for $S = 3/2$. For any half-integer spin value with $D > 0$, the ground state for $B = 0$ is a degenerate Kramers doublet with $S_z = \pm 1/2$. When a magnetic field is applied, no matter what the orientation of B or the magnitude of D, the Kramers doublet splits approximately linearly (for $g\mu_B B < D$), and therefore the Kondo peak position would always undergo an increase that extrapolates to zero for $B = 0$. This is in contradiction to the field dependence that we measure for stretched Co(tpy-SH)$_2$ devices, allowing us to rule out the possibility that $S = 3/2$, or any other half-integer value.

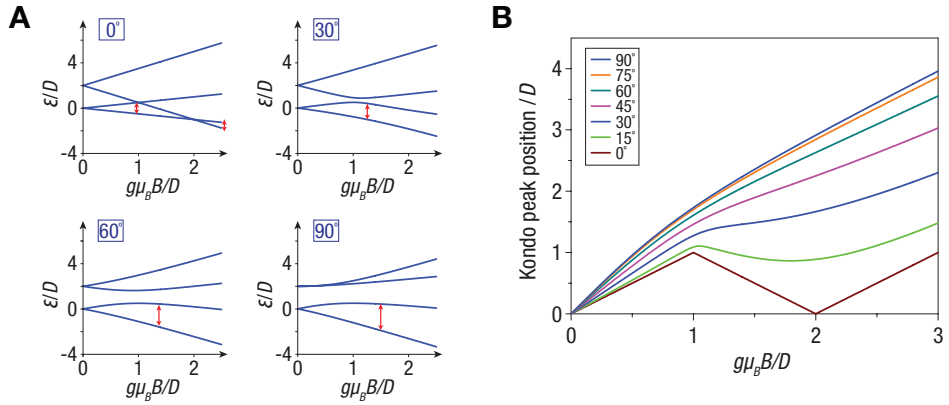

Figure S5: Magnetic field evolution of $S = 3/2$ energy levels in the presence of anisotropy. (**A**) Energy eigenvalues of the model spin-anisotropy Hamiltonian $H = -g\mu_B \mathbf{B} \cdot \mathbf{S} + DS_z^2$ for 4 different field angles with respect to the anisotropy axis. The red arrows indicate the lowest-energy inelastic transitions corresponding to the finite-bias Kondo peaks. (**B**) Predicted Kondo peak position versus magnetic field at several field angles.

S8. Identification of the charge state of the measured Co(tpy-SH)$_2$

We can identify the charge state of the measured Co(tpy-SH)$_2$ complex based on the determination that the ground-state spin is $S = 1$. For a complex in equilibrium with counterions, the metal center would be in the Co^{2+} state with an electronic configuration of $3d^7$ and spin $S = 1/2$ or 3/2 with predominantly $S = 1/2$ at low temperature for this complex [S10], inconsistent with the measured ground state of $S = 1$. Instead, charge transfer of an electron from the gold electrodes to the complex must result in a $3d^8$ Co^{1+} state, which has an $S = 1$ ground state for an approximately octahedral ligand field (Fig. S6A). The other possible low-energy even-electron charge state, Co^{3+}, has $S = 0$ for 6-fold coordinated complexes [S12].

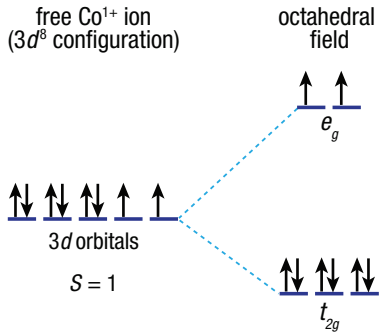

Figure S6: Electronic configuration of the cobalt complex. For a Co^{1+} ion coordinated to ligands with approximately octahedral symmetry, the 5 metal d-orbitals split into a set of t_{2g} and e_g orbitals, and a ground state with $S = 1$ is expected.

S9. Consideration of alternate mechanisms for the stretching-induced Kondo peak splitting

We have considered and can rule out two potential alternative mechanisms for the splitting of the Kondo peak induced by stretching. The "two-stage" $S = 1$ Kondo effect [S15, S16], relevant for temperatures less than the Kondo energy scales for both screening channels (T_{K1} and T_{K2}), can lead to a non-monotonic bias and temperature dependence similar to what we observe in the stretched molecules. However, for this mechanism to explain our data both T_{K2} (reflected in the overall width of the Kondo peak) and T_{K1} would have to increase with stretching. This is unphysical because stretching should weaken the coupling of the metal centre to the electrodes. A splitting of an $S = 1$ Kondo signal could also result from a Jahn-Teller mechanism if distortion caused a non-degenerate $S = 0$ singlet to shift below the $S = 1$ triplet to become the ground state of the molecule. A triplet-singlet crossing has been suggested as the explanation for gate-voltage-induced splittings of Kondo peaks associated with an even number of electrons in GaAs [S17], carbon nanotube [S18], and molecular [S19, S20] quantum dots. However, *ab initio* calculations

indicate that for the range of stretching in our experiment, the $S = 1$ triplet state is always the ground state of Co(tpy-SH)$_2$ (see Section S10). Furthermore, neither a two-stage Kondo effect nor a triplet-singlet crossing would explain the magnetic-field anisotropies that we measure.

S10. Calculations of the triplet-singlet energy gap

We investigated the singlet and triplet energetics of the Co(tpy-SH)$_2^{1+}$ complex with and without attachment to electrodes. Isolated molecule calculations were performed using the ORCA and MOLPRO packages [S14,S21]; molecule-electrode calculations were performed using the VASP package [S22]. We simulated stretching of the molecule in two ways (i) altering the S-S distance, allowing geometric relaxation of the other atoms, and (ii) moving the axial pyridyl moieties in a rigid fashion (see Fig. S7).

Using density functional theory (B3LYP/Def2-TZ2P), we computed the closed-shell (spin-unpolarized) triplet-singlet gap. This tests the Jahn-Teller type scenario mentioned in the previous section – whether mechanical distortion might cause an orbital energy splitting favoring the singlet over the triplet state. We found, however, that both types of stretching lead to the triplet state being below the singlet state by about 0.4 eV (Fig. S8), much larger than any energy scale observed in the experiment. We also carried out multireference complete active space self-consistent field (CASSCF/6-31G) calculations using a 14-electron 14-orbital active space and this yielded a comparable singlet-triplet gap (0.55 eV) near the equilibrium geometry.

Electrodes: To test the effect of attaching to electrodes, we carried out periodic density functional calculations (PAW, 350 eV plane-wave cutoff) with the molecule inserted between two model gold electrodes. Here, pure functionals such as LDA and PBE did not yield magnetization of the molecule in the triplet state, an artifact of the density functional approximations. Moving to the

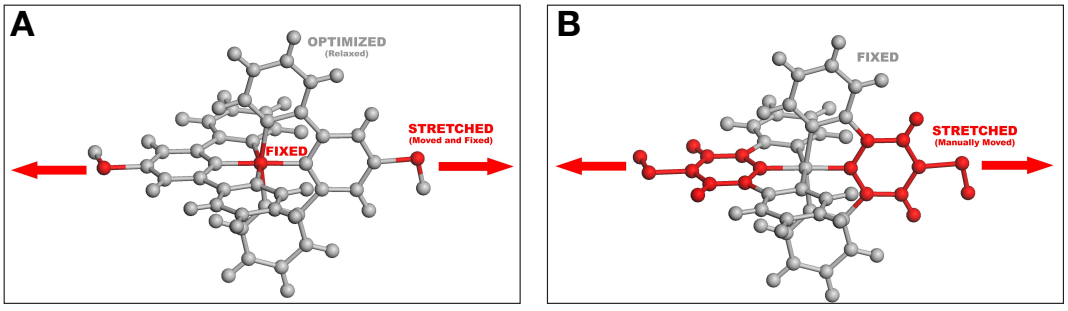

Figure S7: Two simulations of molecule stretching. (**A**) Stretching by increasing the sulfur-sulfur distance while relaxing the positions of the other atoms, and (**B**) stretching by rigidly displacing the axial pyridyls.

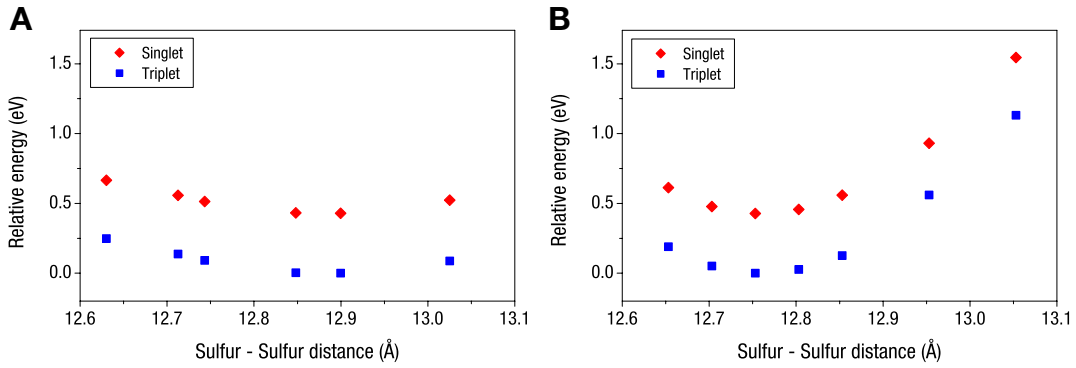

Figure S8: Calculated triplet-singlet energies as a function of stretching obtained by (**A**) varying the sulfur-sulfur distance (with relaxation of the other atoms), and (**B**) rigid displacement of the pyridyl groups. Energies are measured relative to the lowest triplet energy.

LDA + U formalism (Co: $U = 8.0$ eV, $J = 1.0$ eV) [S23] recovered a magnetic cobalt atom in the triplet state, with a corresponding singlet-triplet gap of 0.52 eV at a near-equilibrium molecule-electrode geometry. This appears consistent with our isolated molecule studies.

Other low-lying states: We also investigated the presence of other low-lying states in the spectrum. One possibility is an antiferromagnetic (open-shell) singlet where the cobalt atom is formally Co(III) and the two terpyridine ligands are formally negatively charged with an unpaired electron, antiferromagnetically coupled to each other. In the isolated molecule case, we found the AFM singlet to be lower in energy than the closed-shell singlet. The AFM singlet-triplet gap is very sensitive to the precise theoretical treatment. By varying the amount of exact exchange in the density functional, 0% (BP86), 20% (B3LYP), 50% (BHLYP) we observed gaps of 19.8 meV, 3.1 meV, 1.9 meV. In the case of attached electrodes, we did not find an AFM singlet solution using the LDA and PBE functionals, likely due to the same self-interaction errors in the density functionals that led to the disappearance of the magnetism in the triplet state mentioned above. Nonetheless, we consider it likely that the AFM singlet state may be a low-lying state in these systems.

References

[S1] A. R. Champagne, A. N. Pasupathy, D. C. Ralph, *Nano Lett.* **5**, 305 (2005).

[S2] J. J. Parks *et al.*, *Phys. Rev. Lett.* **99**, 026601 (2007).

[S3] J. Park *et al.*, *Nature* **417**, 722 (2002).

[S4] M.-H. Jo *et al.*, *Nano Lett.* **6**, 2014 (2006).

[S5] H. Park, A. K. L. Lim, A. P. Alivisatos, J. Park, P. L. McEuen, *Appl. Phys. Lett.* **75**, 301 (1999).

[S6] N. Agraït, A. L. Yeyati, J. M. van Ruitenbeek, *Phys. Rep.* **377**, 81 (2003).

[S7] F. Mallet *et al.*, *Phys. Rev. Lett.* **97**, 226804 (2006).

[S8] T. A. Costi, A. C. Hewson, V. Zlatić, *J. Phys. Condens. Matter* **6**, 2519 (1994).

[S9] D. Goldhaber-Gordon *et al.*, *Phys. Rev. Lett.* **81**, 5225 (1998).

[S10] H. A. Goodwin, in *Spin Crossover in Transition Metal Compounds II*, P. Gütlich, H. A. Goodwin, Eds. (Springer-Verlag, Berlin, 2004).

[S11] H. Schoeller, J. König, *Phys. Rev. Lett.* **84**, 3686 (2000).

[S12] A. Abragam, B. Bleaney, *Electron paramagnetic resonance of transition ion*.(Dover Publications, New York, 1986).

[S13] F. Neese, *J. Chem. Phys.* **127**, 164112 (2007).

[S14] ORCA, an *ab initio* DFT and semi-empirical SCF-MO package, version 2.7.-00. F. Neese *et al.*, see `http://www.thch.uni-bonn.de/tc/orca/`.

[S15] W. G. van der Wiel *et al.*, *Phys. Rev. Lett.* **88**, 126803 (2002).

[S16] G. Granger, M. A. Kastner, I. Radu, M. P. Hanson, A. C. Gossard, *Phys. Rev. B* **72**, 165309 (2005).

[S17] A. Kogan, G. Granger, M. A. Kastner, D. Goldhaber-Gordon, H. Shtrikman, *Phys. Rev. B* **67**, 113309 (2003).

[S18] C. H. L. Quay *et al.*, *Phys. Rev. B* **76**, 245311 (2007).

[S19] N. Roch, S. Florens, V. Bouchiat, W. Wernsdorfer, F. Balestro, *Nature* **453**, 633 (2008).

[S20] E. A. Osorio, K. Moth-Poulsen, H. S. J. van der Zant, J. Paaske, P. Hedegård, K. Flensberg, J. Bendix, T. Bjørnholm, *Nano Lett.* **10**, 105 (2010).

[S21] MOLPRO, version 2006.1, a package of *ab initio* programs, H.-J. Werner, P. J. Knowles, R. Lindh, F. R. Manby, M. Schütz, and others, see `http://www.molpro.net`.

[S22] G. Kresse and G. Furthmüller, *Phys. Rev. B* **54**, 11169 (1996).

[S23] V. I. Anisimov, J. Zaanen, and O. K. Andersen, *Phys. Rev. B* **44**, 943 (1991).